Tip-Enhanced Raman Investigation of Extremely Localized Semiconductor-to-Metal Transition of a Carbon Nanotube

Yoshito Okuno,[1] Yuika Saito,[1] Satoshi Kawata,[1,2,3] and Prabhat Verma[1,2]
[1]*Department of Applied Physics, Osaka University, Osaka 565-0871, Japan*
[2]*Photonics Center, Osaka University, Osaka 565-0871, Japan*
[3]*RIKEN, Wako, Saitama 351-0198, Japan*
(Received 25 April 2013; published 19 November 2013)

The electronic properties of single walled carbon nanotubes (SWNTs) can change with a slight deformation, such as the one caused by the pressure of one SWNT crossing over the other in an "*X*" shape. The effect, however, is extremely localized. We present a tip-enhanced Raman investigation of the extremely localized semiconductor-to-metal transition of SWNTs in such a situation, where we can see how the Fano interaction, which is a Raman signature of metallic behavior, grows towards the junction and is localized within a few nanometers of its vicinity. After exploring the deconvoluted components of the *G*-band Raman mode, we were able to reveal the change in electronic properties of a SWNT at extremely high spatial resolution along its length.

DOI: 10.1103/PhysRevLett.111.216101 PACS numbers: 68.37.Uv, 73.63.Fg, 78.30.Na, 78.67.Ch

Tuning the electronic properties of single walled carbon nanotubes (SWNTs) has been a topic of interest for many, particularly those who dream of developing nanoelectronic devices with a variety of electronic characteristics. This surge of interest has given rise to many methods for tailoring electronic properties of SWNTs, such as chemical functionalization [1,2], encapsulation of organic and inorganic materials inside SWNTs, and structural deformation [3]. Theoretical studies have predicted the modulation of electronic bands due to deformation, for example, by bridging them over electrodes [4,5], which was attributed to the π^*-σ^* hybridization occurring near the point of compression [6]. In particular, electronic transport properties measured at the junction constituting two crossed SWNTs showed interesting changes in the conductance at the junction [5,7]. When one SWNT crosses over another, for example in an "*X*" shape (from now on, we will refer them as *X*-CNTs), then both nanotubes can be locally deformed near the junction due to their mechanical interactions via the van der Waals binding of the upper nanotube to the substrate away from the junction. A transformation of SWNTs from semiconductor to metal (S-to-M), invoked by pressure, was theoretically predicted [8] as well as experimentally observed using scanning tunneling spectroscopy [9]. However, the modification of electronic properties has not been observed at high spatial resolution so far, and hence an ambiguity about the extent of such a localized S-to-M transition still exists, which keeps this topic a subject of discussion. An optical technique, such as Raman spectroscopy, can prove to be a suitable tool to study the process of the S-to-M transition in SWNTs, as it enables us to map the physical and electronic properties of a sample simultaneously [10]. However, Raman scattering is a weak phenomenon, and, at the same time, the diffraction limit in confocal Raman measurements inhibits us from obtaining high spatial resolution. Tip enhanced Raman scattering (TERS), on the other hand, not only breaks the diffraction limit but also enhances the scattering by utilizing a sharp metallic nanotip [11–17]. Here in this Letter, we have investigated the vibrational features of *X*-CNTs utilizing TERS spectroscopy and microscopy across the junction at a high spatial resolution.

The semiconducting SWNTs, procured from Meijo Nano Carbon Inc., were spin-casted on a glass coverslip. We then searched for nanotubes laying on one other in the shape of the letter "*X*," using atomic force microscopy (AFM) imaging. As estimated from the height in the AFM line profile, we could find such *X*-CNTs that contained aggregates of 2–3 nanotubes in both branches. It will be demonstrated later that this sample showed similar results as those expected from an *X*-CNT sample containing single nanotubes in each branch. The metallic SWNTs used in the present work were HiPco nanotubes, purchased from Nano Integris. They typically contained some semiconducting impurities. Our TERS experimental setup was based on an inverted optical microscope combined with a contact-mode atomic force microscope. The incident light (cw laser; $\lambda = 488$ nm) was confined and enhanced by a SiO_2 nanotip that was evaporated with a thin layer of silver. The apex of the tip after silver deposition was observed by scanning electron microscope and was confirmed to be 15 nm in diameter. The scattered signal was collected by a high-NA objective lens and the Raman scattered signal was analyzed by a spectrometer. More details of the experimental setup can be found elsewhere [12].

One of the prominent first-order vibrational bands in a typical Raman spectrum of SWNT is the so called *G* band, which contains two distinct Raman modes, a G^- mode and a G^+ mode. In metallic nanotubes, it is believed that the

G^- and the G^+ modes represent the LO and the TO phonons, respectively [18,19]. It has also been known that the conduction electrons in metallic SWNTs couple strongly to the Γ-point LO phonons because each produces a longitudinal field that interacts with the charge density of the other. Since the conduction electrons represent a continuum plasmon and the LO phonons are bound, the interaction is of Fano-type, which results in a shift and an asymmetric broadening of the LO phonon [20–22]. Therefore, the G^- mode contains information related to the electronic properties of the nanotube in the form of asymmetry of the mode. The frequency dependence of Raman intensity in a Fano-type interaction is usually given as [22]

$$I(\omega) = I_0 \frac{\{1 + (\omega - \omega_0)/q\Gamma\}^2}{1 + \{(\omega - \omega_0)/\Gamma\}^2}, \quad (1)$$

where I_0, ω_0, and Γ represent the intensity, renormalized frequency, and broadening parameter, respectively. The parameter q represents coupling between the phonon and the plasmons, and provides asymmetry to the line shape of the G^- mode. For $q = \infty$ or $1/q = 0$, Eq. (1) takes the form of a Lorentzian equation and it refers to a purely symmetric phonon mode. Therefore, the absolute value $|1/q|$, obtained from a Fano curve fitting, can be used as a measure of the degree of S-to-M transition in SWNTs.

Figure 1(a) shows an example of near-resonance far-field Raman spectra in the G-band spectral region from semiconducting and metallic SWNTs. Here, we would like to note that the metallic SWNTs contain a small part of semiconducting nanotubes as impurity. The Raman spectrum of the metallic nanotubes can be best fitted with an asymmetric Fano peak and two symmetric Lorentzian peaks, as shown in Fig. 1(b), where the Fano peak represents the G^- contribution from metallic SWNTs and the weaker Lorentzian peak represents the G^- contribution from semiconducting impurities. The Raman spectrum from semiconducting nanotubes, however, can be best fitted with two symmetric Lorentzian peaks (not shown here). Thus, by observing the asymmetry in the line shape of the G^- mode in a Raman spectrum, one can predict the electronic nature of the nanotube.

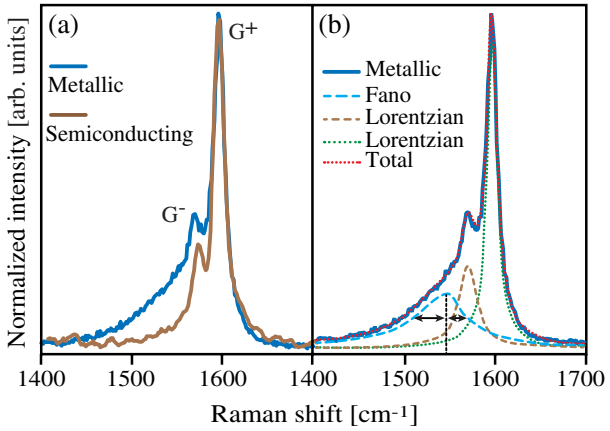

FIG. 1 (color online). (a) Raman spectra of metallic and semiconducting SWNTs presented in blue and brown colors, respectively, in the G-band spectral range. (b) Raman spectrum of metallic SWNTs could be best fitted with an asymmetric Fano peak originating from the G^- mode of the metallic SWNTs and two symmetric Lorentzian peaks, one originating from the G^- mode of the semiconducting impurities and the other from the G^+ mode of all SWNTs.

Figure 2(a) shows a 3D AFM image of our X-CNT sample. The height of each branch was about 2–3 nm, from which we estimate that each branch contains about 2–3 SWNTs. A TERS image, constructed from the peak intensity of the G^+ mode, is shown in Fig. 2(b), where the spatial resolution is 15 nm. Radial breathing modes (RBMs) in the Raman spectra of SWNTs signify the diameters of the nanotubes. TERS spectrum (i) in

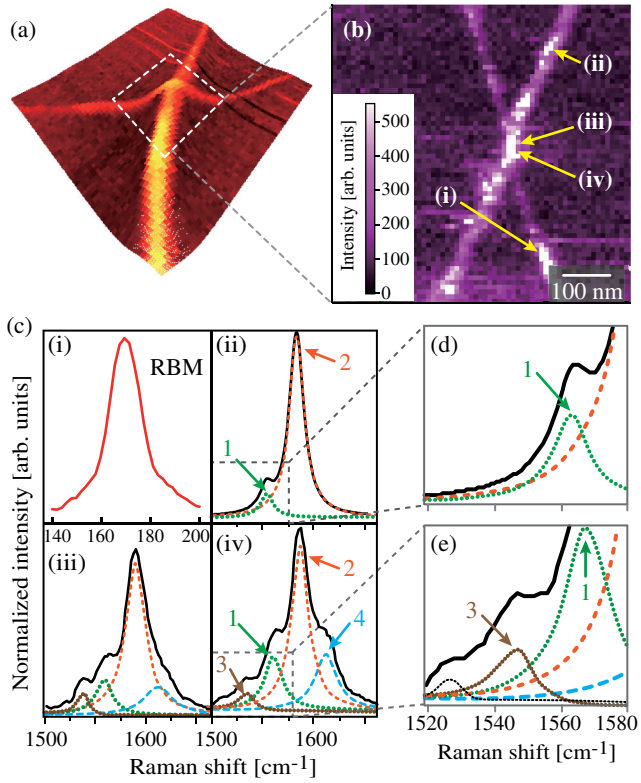

FIG. 2 (color online). (a) A 3D AFM image of our X-CNT sample. (b) G^+ mode TERS image of the sample area enclosed by the white dashed line in (a). (c) TERS spectra obtained from points (i) through (iv) indicated in (b). Spectrum at point (i) shows the RBM region with the presence of only one peak. The G-band spectrum obtained far from the junction at point (ii) could be decomposed into two symmetric Lorentzian peaks (peak 1 and peak 2), while the spectra obtained near the junction at points (iii) and (iv) required two additional peaks, one asymmetric Fano peak (peak3) and one symmetric Lorentzian peak (peak 4) for the best fitting. (d) and (e) show magnified Raman spectra obtained far from the junction and near the junction, respectively.

Fig. 2(c), which was measured far from the junction at point (i) marked in Fig. 2(b), shows that only one RBM at 169 cm^{-1} could be observed, which corresponds to a diameter of 1.4 nm [23]. Further, TERS spectra obtained in the G-band spectral region from three different points, as indicated by the points (ii) through (iv) in Fig. 2(b), are also shown in Fig. 2(c). A careful observation of these spectra reveals that the spectrum obtained far from the junction at point (ii) could be best fitted with two Lorentzian curves centered at 1565 and 1588 cm^{-1}, representing the G^- and G^+ modes of semiconducting SWNTs, respectively. We will call these peaks peak 1 and peak 2, which are also marked in the figure. On the other hand, the spectra obtained near the junction at points (iii) and (iv) required two extra curves for the best fitting, one Fano curve centered at 1548 cm^{-1} and one Lorentzian curve centered at 1607 cm^{-1}, which we will call peak 3 and peak 4, respectively. For clarity, Figs. 2(d) and 2(e) show zoomed displays for the spectra obtained at points (ii) and (iv), respectively. Here, we note that some times a small peak around 1525 cm^{-1} was observed, as shown in 2(e), the origin of which is not clear. It could be a deformation-activated peak, nevertheless, the asymmetry in peak 3 can still be clearly observed in the presence of this peak.

It is clear from Fig. 2(c) that the G-band spectral shape is significantly changed around the junction. A quick comparison with Fig. 1 reveals that the nanotubes at a location far from the junction are semiconducting, while the same nanotubes at a location near the junction show a combination of both metallic and semiconducting characters. There are two interesting differences in the spectra obtained near the junction. The first is the appearance of an asymmetric Fano peak, and the second is the presence of new additional modes. Indeed, both the Fano and the new peaks arise from the fact that the nanotubes are locally deformed at the junction. On one hand, the deformation modifies the electronic properties near the junction resulting in a localized S-to-M transition, which gives rise to a Fano-type peak. On the other hand, the deformation locally destroys the radial symmetry of the nanotubes at the junction and thus the selection rules are relaxed and additional phonons become observable in Raman scattering. The deformation extends to a length smaller than the size of the confined light at the tip apex; therefore, a TERS spectrum measured right at the junction contains contributions from both deformed and nondeformed areas of the nanotubes. Additionally, as there are 2–3 nanotubes in each branch, there is a possibility that some nanotubes at the junction do not get deformed. The signal from such nondeformed nanotubes may also contribute to the total Raman signal. The appearance of four peaks at the junction can be thus explained as follows. Peak 1 and peak 2 originate from the unperturbed or nondeformed part of the nanotubes immersed within the confined light. Peak 3 originates from the local metallic character of the nanotubes deformed at the junction. The Fano interaction, as defined in Eq. (1), shifts the G^- mode towards lower frequency, which causes peak 3 to show up distinctly at a shifted frequency compared to peak 1. Finally, peak 4 is the new Raman mode observed due to the reduction in radial symmetry at the junction, which is not observable under total radial symmetry. The existence and the location of this peak are in good agreement with a previous report, where the authors concluded that symmetry breaking can result in the observation of several new Raman modes in the G-band spectral range [24]. In the present case, we observe only one additional peak.

Even though our X-CNT sample in Fig. 2 contains 2–3 aggregated nanotubes in each branch, the phenomenon of the localized S-to-M transition at the junction is identical to what is expected for a sample with single nanotubes in each branch. In order to establish our point, we demonstrate similar measurements in Fig. 3, which were performed on an X-CNT sample containing single nanotubes in each branch. Figure 3(a) shows an AFM image of the sample, and Fig. 3(b) shows a line profile along the white dashed line in Fig. 3(a). The line profile confirms that both branches of the X-CNT sample contain single nanotubes with a diameter of 1.5 nm, which is close to the value that we estimated from the RBM (1.4 nm). TERS spectra measured in the G-band spectral region at the junction and far from the junction are shown by (i) and (ii), respectively, in Fig. 3(c). The curve fittings show that the spectrum measured near the junction at point (i) can be best fitted with one Fano curve and three Lorentzian curves, while the spectrum measured far from the junction at point

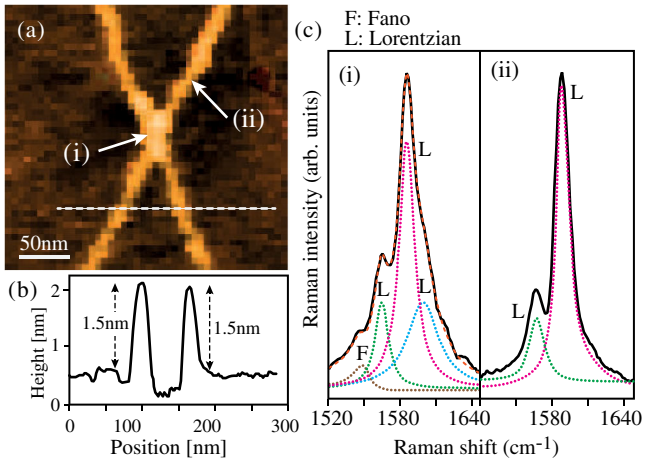

FIG. 3 (color online). (a) AFM image of an X-CNT sample consisting of single nanotubes in each branch. (b) A line profile along the white dashed line confirming the diameter of the nanotubes is about 1.5 nm. (c) TERS spectrum in the G-band region measured from point (i) at the junction and point (ii) far from the junction. Similar to Fig. 2, the spectrum far from the junction can be fitted with two Lorentzian curves, while the spectrum at the junction requires one additional Lorentzian curve and one Fano curve for the best fitting.

(ii) can be best fitted with two Lorentzian curves. We measured TERS spectra along both branches of the sample at several points away from the junction and confirmed that the sample shows semiconducting characteristics everywhere except at the junction. This result is identical to what we have observed in Fig. 2, confirming that even though the sample in Fig. 2 contained 2–3 nanotubes in each branch, this small aggregation did not affect our analysis about the localization of deformation and electronic properties of the SWNTs. However, the sample in Fig. 3 shows weaker scattering and requires more than 90 min of measurement time for TERS imaging. This measurement time is too long for our system to be perfectly stable under ambient conditions even with a feed-back system. On the other hand, the TERS image in Fig. 2 requires only about 20 min, for which our system shows no drift. We would therefore continue our further analysis using the sample in Fig. 2, noting that we expect the same results for a sample having single nanotubes in each branch.

In order to understand the localization of the modified electronic property, we decomposed TERS spectra obtained from the entire X-CNT sample in Fig. 2 into Fano and Lorentzian curves. As expected, the Fano parameter $|1/q|$ was found to be zero at all points far from the junction. On the other hand, $|1/q|$ varied from 0.2 to 0.4 near the junction confirming a significant amount of phonon-plasmon coupling around the junction. The maximum value of $|1/q|$ has been reported to be 0.4 [25,26], which indicates that the SWNTs at the junction turn completely into metallic SWNTs. Figure 4(a) shows a TERS image of the X-CNT sample, where the z axis represents $|1/q|$. A strong localization of $|1/q|$ can be confirmed around the junction by a sharp peak seen in the z direction. In addition, Fig. 4(b) shows a line profile (FWHM = 15 nm) along the yellow dashed line marked in Fig. 4(a), confirming a strong localization of the S-to-M transition in the sample. It has been theoretically predicted for flattened SWNTs that such a S-to-M transition could be localized to a much smaller length [27]. However, we cannot distinctly measure the confinement beyond the spatial resolution of our TERS system.

Next, we investigated the new mode, peak 4, which appears due to the local reduction of radial symmetry. Figures 4(c) and 4(d) show the spatial confinement of this mode. The white dashed lines in Fig. 4(c) depict the location of the sample and the colored dots indicate the intensity of peak 4. As one can see here, the intensity of peak 4 is strong only in the very close vicinity of the junction. This result is also displayed in Fig. 4(d), where the peak intensity is plotted with respect to the distance measured from the junction. Figures 4(c) and 4(d) clearly show that the distortion and the reduction of symmetry are strongly localized near the junction.

In summary, by utilizing our state-of-the-art TERS spectroscopy and microscopy techniques, we have investigated an X-CNT sample to reveal the phenomenon of the S-to-M transition that occurs at the extremely localized area of the sample near the junction. This was observed through the appearance of the Fano interaction between the plasmon and phonon. At the same time, we have also discovered that new Raman modes appear in the same area near the junction, confirming extremely localized physical distortion of the nanotubes due to the pressure applied on one nanotube by the other. The modification of electronic properties, as well as the physical distortion, takes place within a length smaller than 15 nm. The present results could be very interesting for CNT-based device fabrication where the local modification of electronic properties could play an important role.

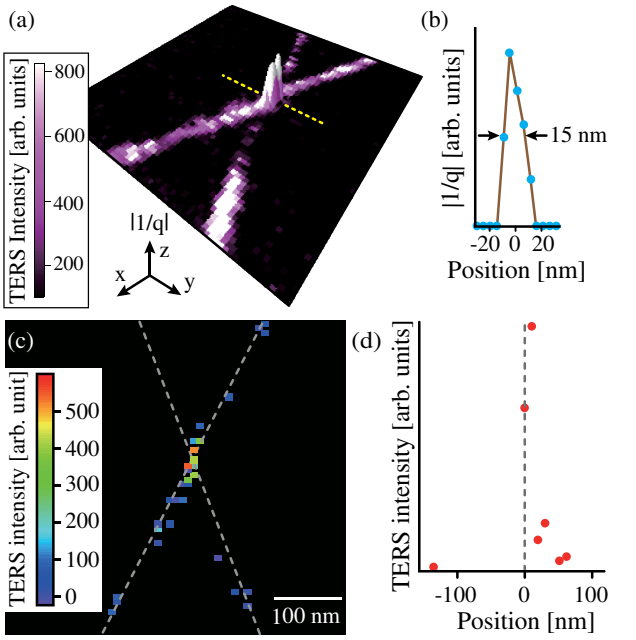

FIG. 4 (color online). (a) A TERS image of our X-CNT sample, where x and y axes show the sample plane, the color represents TERS intensity of the G^+ mode in accordance with the color bar shown on the left, and the z axis shows the value of $|1/q|$. (b) A line profile of $|1/q|$ along the yellow dashed line in (a). (c) White dashed lines depict the location of the nanotubes in the X-CNT sample, whereas the colored spots indicate the TERS intensity of peak 4, in accordance with the color bar on the left. (d) TERS intensity plotted along one branch of the nanotube across the junction showing sudden increase in intensity at the junction.

This work was supported by the Japan Society for the Promotion of Science (JSPS) under the Asian Core project. The authors would like to thank T. Yano of Tokyo Institute of Technology for helpful discussions.

[1] Z. Liu, C. Davis, W. Cai, L. He, X. Chen, and H. Dai, Proc. Natl. Acad. Sci. U.S.A. **105**, 1410 (2008).
[2] M. S. Strano, C. A. Dyke, M. L. Usrey, P. W. Barone, M. J. Allen, H. Shan, C. Kittrell, R. H. Hauge, J. M. Tour, R. E. Smalley, Science **301**, 1519 (2003).

[3] T. W. Tombler, T. W. Tombler, C. Zhou, L. Alexseyev, J. Kong, L. Liu, C. S. Jayanthi, M. Tang, and S.-Y. Wu, Nature (London) **405**, 769 (2000).
[4] T. Hertel, R. E. Walkup, and P. Avouris, Phys. Rev. B **58**, 13 870 (1998).
[5] H. W. Ch. Postma, M. de Jonge, Z. Yao, and C. Dekker, Phys. Rev. B **62**, R10653 (2000).
[6] X. Blase, L. Benedict, E. Shirley, and S. Louie, Phys. Rev. Lett. **72**, 1878 (1994).
[7] M. S. Fuhrer *et al.*, Science **288**, 494 (2000).
[8] B. Shah, G. W. Lakatos, S. Peng, and K. Cho, Appl. Phys. Lett. **87**, 173109 (2005).
[9] L. Vitali, M. Burghard, P. Wahl, M. Schneider, and K. Kern, Phys. Rev. Lett. **96**, 086804 (2006).
[10] A. Jorio, M. A. Pimenta, A. G. S. Filho, R. Saito, G. Dresselhaus, and M. S. Dresselhaus, New J. Phys. **5**, 139 (2003).
[11] A. Hartschuh, E. Sánchez, X. Xie, and L. Novotny, Phys. Rev. Lett. **90**, 095503 (2003).
[12] P. Verma, K. Yamada, H. Watanabe, Y. Inouye, and S. Kawata, Phys. Rev. B **73**, 045416 (2006).
[13] T. Ichimura, S. Fujii, P. Verma, T. Yano, Y. Inouye, and S. Kawata, Phys. Rev. Lett. **102**, 186101 (2009).
[14] T. Yano, P. Verma, Y. Saito, T. Ichimura, and S. Kawata, Nat. Photonics **3**, 473 (2009).
[15] S. Kawata, Y. Inouye, and P. Verma, Nat. Photonics **3**, 388 (2009).
[16] P. Verma, T. Ichimura, T. Yano, Y. Saito, and S. Kawata, Laser Photonics Rev. **4**, 548 (2010).
[17] J. Yu, Y. Saito, T. Ichimura, S. Kawata, and P. Verma, Appl. Phys. Lett. **102**, 123110 (2013).
[18] M. Lazzeri, S. Piscanec, F. Mauri, A. Ferrari, and J. Robertson, Phys. Rev. B **73**, 155426 (2006).
[19] S. Piscanec, M. Lazzeri, J. Robertson, A. Ferrari, and F. Mauri, Phys. Rev. B **75**, 035427 (2007).
[20] U. Fano, Phys. Rev. **124**, 1866 (1961).
[21] V. Klein *et al.*, in *Light Scattering in Solids I*, edited by M. Cardona (Springer-Verlag, Berlin, 1983), pp. 169–172.
[22] A. M. Rao, A. M. Rao, S. Bandow, A. Thess, and R. E. Smalley, Nature (London) **388**, 257 (1997).
[23] H. Kataura, Y. Kumazawa, Y. Maniwa, I. Umezu, S. Suzuki, Y. Ohtsuka, and Y. Achiba, Synth. Met. **103**, 2555 (1999).
[24] Y. Ren, L. Song, W. Ma, Y. Zhao, L. Sun, C. Gu, W. Zhou, and S. Xie, Phys. Rev. B **80**, 113412 (2009).
[25] K. T. Nguyen, A. Gaur, and M. Shim, Phys. Rev. Lett. **98**, 145504 (2007).
[26] S. D. M. Brown, A. Jorio, P. Corio, M. Dresselhaus, G. Dresselhaus, R. Saito, and K. Kneipp, Phys. Rev. B **63**, 155414 (2001).
[27] M. S. C. Mazzoni, and H. Chacham, Appl. Phys. Lett. **76**, 1561 (2000).